Maritime Technology and Engineering 3 – Guedes Soares & Santos (Eds)
© 2016 Taylor & Francis Group, London, ISBN 978-1-138-03000-8

CFD assessment of Ropax hull resistance with various initial drafts and trim angles

J. Labanti, H. Islam & C. Guedes Soares
Centre for Marine Technology and Ocean Engineering (CENTEC), Instituto Superior Técnico, Universidade de Lisboa, Lisbon, Portugal

ABSTRACT: A Ropax hull resistance has been studied with OpenFOAM considering different Froude numbers, trim angles and drafts. The simulations have been set in calm water, model scale, using a multiphase domain implemented with a volume-of-fluid method and a SST k-ω turbulence model. The first simulation has been run even keel at design draft, Fr = 0.2, both with the hull fixed in its original position and with the hull free to sink and trim. Comparison of results with another RaNS code has been also performed. Next, systematic data collection has been done with the hull fixed in various particular positions, at Fr = 0.20. Similar simulations at higher Fr numbers have been run; in these cases a coarser mesh has been used in order to achieve a less request of computational power and a more stable behavior.

1 INTRODUCTION

In order to predict the ship's resistance and, as a consequence, the ship's consumption in an early stage of design, CFD has become an increasingly reliable and powerful tool. Several studies about using this tool for ship hull optimization have been done, as described by Percival et al (2001), Campana et al (2006) and Peri et al (2001).

Furthermore, ship resistance is not only related to the shape of the hull, but also depends on dynamic effects like sinkage and trim developed during navigation. It follows the importance of predicting properly these motions: a possible basic CFD setup to study the problem is explained by Yang et al (2000) whereas Carrica et al (2011) go further implementing a self-propelled model free to sink and trim. Similar investigations have been done by Wortley (2013) on a container ship and by Tarbiat et al (2014) on the Wigley hull, and they have been the references for the work presented here.

Particularly, the Ropax object of these paper is a kind of ship where resistance shifts considerably due to dynamic effects combined with loading conditions as shown by data recorded on operating ship by Galli et al (2014).

In order to reproduce numerically these situations, OpenFOAM has been used. It is a C++ open source software where a Reynolds Average Navier Stokes set of equations has been implemented in the finite volume scheme, plus the two equations of the SST k-ω turbulence model to close numerically the problem. ITTC guidelines (2011) and Ciortan et al (2012) have been followed for the model setup. Turbulence parameters have been calculated using the most common formulas; simulations at Fr = 0.2 have shown convergence whereas the ones at higher Fr numbers have shown problems, producing wave form the inlet. This problem is also reported in Ciortan et al (2007) and has been partially avoided using different solver, changing pressure boundary conditions at the outlet and inserting coarser mesh zones near the sides and at the outlet like pointed by Yang et al (2011); however, further investigations in this field are required.

Even though there aren't towing tank data as benchmark, comparison with a well validated RaNS code has been done and data from numerical simulations reported here represent nevertheless interesting insights about trim and draft effects.

Firstly, an even keel resistance evaluation has been performed to test the software; insights by Maki (2011), Maki et al (2013) and Ahmed et al (2009) have been followed. Then, after an initial comparison between the even keel resistance calculated with the hull fixed in its original position and the hull free to sink and trim, likewise Hajivand and Mousavizadegan (2015), the present paper shows the results of the resistance calculation at design draft with different initial trims, Fr = 0.2, using a static mesh.

The considered trims are weighted average of the most common angles a Ropax can reach due to dynamic effects combined with loading conditions. Trim angles are included in a range from 0.4° by stern to 0.2° by bow, step 0.2°. Furthermore, the resistance's dependence from draft has been studied. Simulations even keel with different drafts have been run: design draft, minimum draft allowed and intermediate draft between the former two values have been considered. At higher Fr numbers the same investigations of trim and draft showed problems and the

Table 1. Ship data, model scale.

	Ship scale	Model scale
L_{pp}, m	90	3.600
B_{wl}, m	17.82	0.713
Tdesign, m	4	0.168
D, m	14.8	0.592
∇, m^3	3725	0.238
S, m^2	1743	2.788
Cb	0.55	0.55
Awl, m^2	1311	2.097
xG, m	−3.5	−0.14
GML, m	170	10.152

setup able to avoid them does not produce reliable results.

The final purpose of this paper is describing how this open source software can be used in an early design stage, obtaining a rough idea of the ship behavior in terms of relationship between resistance, pitch angles and drafts with no license costs and less request of computational power.

2 SHIP DATA AND REFERENCE SYSTEM

The Ropax object of the simulation is a monohull whose main data are reported in Table 1.

It is fitted with skeg and has no bulbous bow. It also has two four-bladed counter-rotating (inwards) propellers and it's equipped with two Becker flap spade rudders.

For the resistance computation only bare hull and skeg were considered. Furthermore, only few data of this ship were available; the hydrostatic features such as the position of the centre of buoyancy (B) and the wet surface have been calculated from the IGES model, whereas the centre of gravity position (G) is unknown. Due to lack of data, G has been set in the same longitudinal position as B in order to have equilibrium at pitch. Ship is upright in every simulation. G height has been set at D/2, but the vertical position of G is useful only when dealing with dynamic mesh to evaluate the constraint in pitch (C55 in linearized equation of motion). C55 is function of GML, but KML is much more higher than KG, so it's been considered a reasonable approximation.

The origin of the reference system used in OpenFOAM to construct the domain and calculate the G and B position is placed as follows:

- Ox: PP1/2, x positive forward
- Oy: symmetry plane, y positive portside
- Oz: waterplane, z positive upward

Simulations have been run in model scale (1:25) to reduce the required computational power. This, according to Jin et al (2016) leads to consistent errors when calculating hydrodynamic manoeuvering coefficients (10% to 30%) whilst scale effects lead to errors below 8% for surge force; for this reason model scale simulations have been considered a reasonable approximation.

Figure 1. Reference system.

All forces and moments are referred to a system parallel to the reference one but centered in G; that's irrelevant for the resistance calculation but it counts for the moment around y-axis.

3 MODEL SETUP

The paper mainly focuses on OpenFOAM to predict trim effect on ship resistance. Given that no experimental data was available for proper validations, the initial results have been compared to simulation results produced by another RaNS solver, SHIP_Motion. The mathematical model of the solver has been elaborately discussed by Orihara et al. (2003), and Kim et el. (2015) in their works, respectively. The solver has been validated for several ship models previously.

3.1 OpenFOAM

The domain size for OpenFOAM simulation has been set following ITTC (2011) guidelines and the work by Shi et al (2012): the inlet has been placed one ship length windward the bow, the outlet five Lpp downstream the stern; each lateral boundary is two ship lengths away from the ship's symmetry plane.

The bottom has been placed at a sufficient distance from the free surface in order to avoid interactions with the generated wave pattern and reproduce a deep water condition: one ship length is enough to achieve it. The atmosphere has been placed at 0.5 L above the free surface.

Mesh has been generated using snappyHexMesh utility, which creates automatically a "body fitted" hexahedral mesh from an STL surface, following suggestion by Jackson (2012).

A mesh refinement across the free surface has been performed in order to have at least 40 cells per expected wavelength. The height of the first cell inside the expected boundary layer has been estimated for $y+ = 1$; the max cell height has been calculated instead for $y+ = 50$ and corresponds approximatively to the beginning of the logarithmic region.

In order to damp the outgoing waves and, hopefully, prevent making waves from the inlet a sponge layer zone should have been necessary as pointed by Yang et al (2011) and Hu et al (2015): however, only a coarser mesh near the sides of the block has been sufficient instead of proper "numerical beaches" based on relaxation method. Thanks to this artificial damping, incoming waves have been avoided for $Fr = 0.2$.

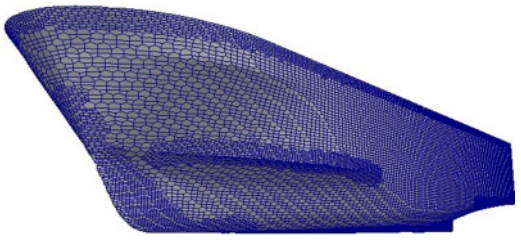

Figure 2. Hull mesh.

Table 2. Mesh quality.

Fr	0.20	0.25/0.30
Points	1.4 mln	800 k
Faces	4 mln	226 k
Cells	1.3 mln	223 k
Hexahedra	1.25 mln	730 k
Prisms	2 k	700
Polyhedra	58 k	36 k

This problem is still present for higher Fr numbers considered here, so a different set up has been implemented. The pressure boundary condition at the outlet has been changed in order to force the wave damping, and interFoam instead of LTSInterFoam has been used due to its more stable behaviour. This set up has less physical sense and the results seem to be less reliable. A coarser mesh has been used to save computational time.

3.1.1 *Turbulence parameters*

Turbulence has been modelled with a Reynolds-averaged stress (RAS) SST *k-ω* two equation model. The parameters have been calculated following the most common guidelines as follows:

$$I = 0.16 \cdot Re^{-1/8} \tag{1}$$

$$k\,[\frac{m^2}{s^2}] = \frac{3}{2}(u \cdot I)^2 \tag{2}$$

$$\delta\,[m] = \frac{L}{\sqrt{Re}} \tag{3}$$

$$l\,[m] = 0.4 \cdot \delta \tag{4}$$

$$C\mu = 0.09 \tag{5}$$

$$\omega\,[\frac{1}{s}] = \frac{\sqrt{k}}{C_\mu{}^{1/4} \cdot l} \tag{6}$$

$$\nu_T\,[\frac{m^2}{s}] = \sqrt{\frac{3}{2}} \cdot u \cdot I \cdot l \tag{7}$$

where I is the turbulence intensity, analytically defined as the ratio between the root-mean-square of the turbulent velocity fluctuations and the mean velocity; k is the turbulent kinetic energy per unit mass; δ is the height of the boundary layer; l is the turbulence length scale, describing the size of the large energy-containing eddies in a turbulent flow; Cμ is an empirical constant; ω is the turbulence specific dissipation rate; and ν T is the turbulent kinetic eddy viscosity.

Table 3. Physical constants.

	Water	Air
ρ, kg/m^3	1000	1
ν, m^2/s	1.09e−06	1.48e−05

Table 4. Boundary conditions.

	Inlet	Outlet	Atmosphere	Hull
U	FV	ZG	PIOV	MWV
p_rgh	FFP	ZG	TP	FFP
α.water	FV	ZG	IO	ZG
k	FV	ZG	IO	kqRWF
nut	FV	ZG	ZG	nutkRWF
omega	FV	IO	IO	omegaWF

The density and the kinematic viscosity of the fluids used in simulations are reported in Table 3.

3.1.2 *Boundary conditions*

The control volume represents a deep water condition, so the two lateral sides and the bottom are symmetry plane type faces; no additional information is required for this kind of boundary condition. Inlet, outlet and atmosphere are patch faces with specific boundary condition for each one, whilst hull is a wall type one. Boundary condition setting is based on Wortley (2013), Mordhorst (201), Yang et al (2011). For the Fr = 0.2 case boundary conditions are as follow:
Where:

- FV is fixedValue, specified by the user
- ZG is zeroGradient
- FFP is fixedFluxPressure, that adjusts the pressure gradient such that the flux on the boundary is that one specified by the velocity boundary condition
- PIOV is pressureInletOutletVelocity, that applies zero-gradient for outflow, whilst inflow velocity is the patch-face normal component of the internal-cell value.
- TP is totalPressure, calculated as static pressure reference plus the dynamic component due to velocity
- IO is inletOutlet, that provides a zero-gradient outflow condition for a fixed value inflow
- MWV is movingWallVelocity. This condition has been placed for dynamic mesh, but it also works with static mesh (in this case the velocity is simply zero)
- WF is wallFunction, and each turbulence parameter has its own.

For the higher Fr numbers, p_rgh outlet boundary condition (zeroGradient) has been replaced with

Table 5. Internal fields initial values.

	IF type	IF value	unit
U	uniform	−U	m/s
p_rgh	uniform	0	Kg/ms^2
α.water	uniform (setFields)	0/1	–
k	uniform	(2)	m^2/s^2
nut	uniform	(7)	m^2/s
omega	uniform	(6)	1/s

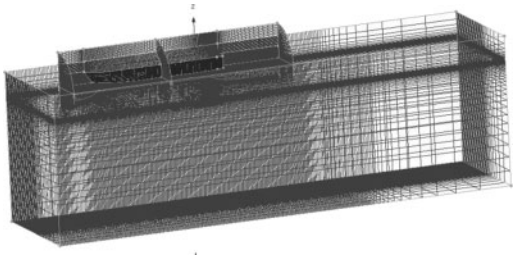

Figure 3. Overset mesh structure for SHIP_Motion.

fixedValue (0) in order to force the damping of the Kelvin pattern.

3.2 *SHIP_Motion model*

For running simulation using SHIP_Motion, an overset structured mesh system has been used (Figure 3). The coarse rectangular outer mesh with high resolution around the free surface has been used to capture the free surface deformation. The fine O-H type inner mesh around the hull surface has been used for capturing the flow properties around the hull surface. The mesh has been generated using commercial mesh generation tool Pointwise.

SHIP_Motion being a dedicated solver for ship hydrodynamic simulation requires limited input data for running simulation. Thus, most of its boundary conditions and solver modeling are pre-defined. The solver just requires basic geometric information of the ship model and the applied Reynolds and Froude number. All simulations are ran in non-dimensional scale. The simulation conditions and mesh resolution are in Table 6 and Table 7 respectively.

4 SOLVERS

4.1 *OpenFOAM*

All considered solvers (interFoam, LTSinterFoam and interDyMFoam) work with the PIMPLE algorithm. The first simulation has been run even keel both with a static hull and with a dynamic hull able to translate along z-axis and rotate around y-axis. For the static hull LTSInterFoam has been used, where LTS means local-time stepping: it manipulates the time step for each individual cell in the mesh, making it as high as

Table 6. Simulation setup used in SHIP_Motion.

Fr	0.20
U, m/s	5.9427
Re	4.907e08
DOF	Heave and pitch

Table 7. Mesh resolution used in SHIP_Motion.

	Inner mesh	Outer Mesh
Length in x-direction (n° of cells)	1.85 L (171)	3.8 L (192)
Length in y-direction (n° of cells)	0.30 L (27)	1 L (45)
Length in z-direction (n° of cells)	0.30 L (66)	1.2 L (63)

*L = Ship length.

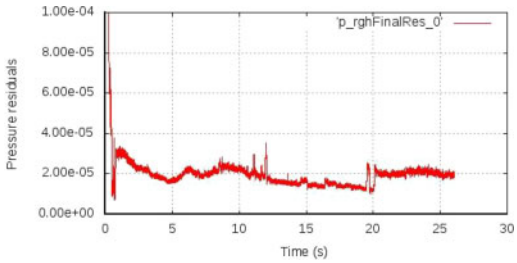

Figure 4. Residuals checking, Fr = 0.2, LTSInterFoam.

possible to enable the simulation to reach steady-state quickly. LTSInterFoam first maximizes the time-step according to the local Courant number, then processes the time-step field by smoothing the variation in time step across the domain to prevent instability due to large conservation errors caused by sudden changes in time step. This approach works very well for low Fr whereas for higher Fr numbers contributes to the problem explained in section 3 and leads to divergence.

In the static hull case, the expected dynamic sinkage and trim have been calculated from the global z-force and y-moment acting on hull with following formulas, under the hypothesis that the ship's sides are vertical and displacements are small:

$$Squat\ [m] = \frac{|Fz - \rho g \nabla|}{\rho g A w l} \tag{8}$$

$$\text{Trim}\ [rad] = \frac{My}{\rho g I y} \tag{9}$$

where *Fz* is the total force in z direction around the hull; *My* total moment around y-axis; *Iy* is the moment of inertia of the waterplane around y-axis. Trim is positive by bow.

For the dynamic mesh case interDyMFoam has been used. The area interested by the mesh movement has

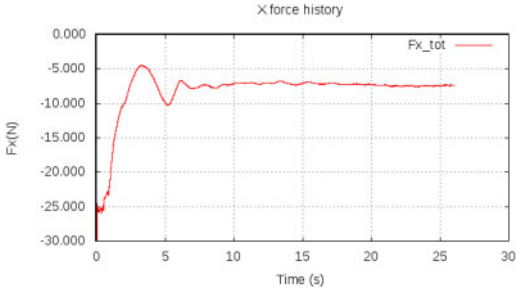

Figure 5. Resistance time history, Fr = 0.2, LTSInterFoam.

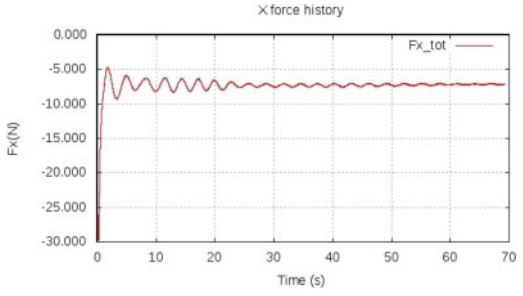

Figure 6. Trim time history, Fr = 0.2, interDyMFoam.

been set as a vertical cylinder of one Lpp radius centred in the origin of the reference system. Hull's centre of mass, mass moments of inertia and constraints have also been specified in the relative dynamic mesh dictionary. Dynamic trim and sinkage have been checked run-time from the log of the simulation. For both the solvers the maximum time step has been set as function of the flow velocity (0.001·L/U) and the maximum Courant number has been set as 0.9.

The simulations have shown convergence that has been checked run-time with the x-force and the dynamic pressure residuals histories (Figure 4). To achieve convergence, about 800 CPU hours are required, equal around 25 seconds of simulation; more time is needed in case of interDyMFoam, as seen in Figure 6, due to oscillations around dynamic equilibrium position.

4.2 *SHIP_Motion*

The governing equation for the mathematical model of SHIP_Motion is the Reynolds averaged Navier-Stokes (RaNS) equation and continuity equation. Two sets of coordinate system, body fixed and earth fixed, have been used. The spatial discretization is by Finite Volume Method (FVM). 3rd order upwind differencing has been used for advection, whereas, discretization in space is by 2nd order central difference scheme. Definition of flow variables are in staggered manner. Free surface capturing is by Marker density method, where, 3rd order upwind scheme performs space differencing and 2nd order Adams-Bashforth solves time differencing. Two type of turbulence models have been incorporated, Baldwin-Lomax and Dynamic subgrid scale model. Wall function has been used to reduce dependency on mesh for capturing boundary layer properties. Parallel processing is by the shared memory model of OpenMP.

Table 8. Results comparison between the two solvers.

	Static mesh LTSInterFoam	Dynamic mesh interDyMFoam	Dynamic mesh SHIP_Motion
Fr	0.20	0.20	0.20
U, m/s	1.1885	1.1885	5.9427
Time step	Fixed (1e−3)	Adjustable	Fixed (1e−4)
Cells	1328903	1328903	849042
Iterations	15000	65000	50000
CT	3.631e−03	3.634e−03	3.370e−03
Sinkage, %	0.60	1.5	2.16
Trim, deg	0.104	0.109	0.12

A Marker and Cell (MAC) type pressure solution algorithm has been employed. The pressure is obtained by solving the Poisson equations using the SOR method and velocity components are gained by correcting the velocity predictor with the implicitly evaluated pressure. In the overlapping grid system, inner domain moves according to floating body's equation of motion and outer domain represents free surface. Grid points located at the overlapping region exchange information through interpolation to update both the domains at every time step.

The solver runs simulation in non-dimensional scale and the results are later converted to dimensional scale. For calm water simulation, only half-hull has been considered, but following results presented here are referred to the full hull for consistence with OpenFOAM data.

5 RESULTS AT FR = 0.20

The first simulation has been run at design draft, even keel and Fr = 0.2 to compare the behavior of the two solvers of OpenFOAM and the other RaNS code. Resistance and sinkage are presented here in a non-dimensional form as follows:

$$CT = \frac{|Fx|}{0.5\rho SUmean^2} \tag{10}$$

$$Squat\ [\%] = 100 \cdot \frac{Squat}{T} \tag{11}$$

The resistance calculated by each solver are comparable, but as seen in the figures above LTSInterFoam reach convergence quickly: 15000 iterations against the 65000 required by interDyMFoam. This happens because the dynamic mesh, during its run, fluctuates around its equilibrium position, as shown both from the x-force (Figure 6) and trim (Figure 7). At the end of the

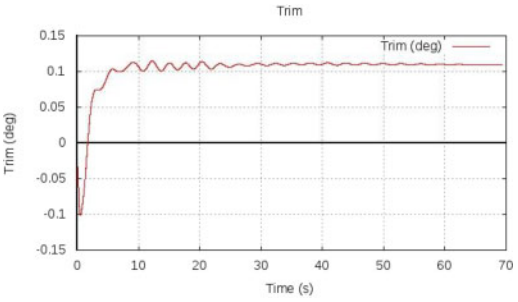

Figure 7. Trim time history, Fr = 0.2, interDyMFoam.

Table 9. CT as function of Fr and initial trim.

Initial trim deg	Fr = 0.20
−0.4	3.905e−03
−0.2	3.742e−03
0.0	3.631e−03
0.2	3.750e−03

runs, the CT difference between the two approaches is about 0.08% and the difference with SHIP_Motion is below 7%. However, the static mesh approach doesn't allow the proper evaluation of the expected dynamic effects due to the flow: sinkage calculated form the global z-force in the static mesh method is less than the half of the one obtained by the dynamic mesh approach as well as from SHIP_Motion.

Anyhow, CFD in general is not very accurate in predicting sinkage, as it is highly mesh dependent. Thus, although there is difference between predictions of different solvers, the results give a rough idea regarding the sinkage of the ship.

Trim obtained by the two OpenFOAM solvers are very close, with the one obtained by SHIP_motion being slightly lower with a difference of 10%. Overall, since, results from both the OpenFOAM solvers and SHIP_motion are in good agreement, it may be concluded that the results predicted here are reliable.

5.1 *Trim effects*

The initial trim angles have been chosen as reasonable angles, the ship can have due to its loading conditions and dynamic effects during navigation. For each condition the wet surface has been considered the same as the even keel one.

A second order dependence of the resistance from the trim has been observed, with the minimum value for the even keel situation. Polynomial fit has been constructed for CT dependence from trim, as shown in Eq. (12).

$$CT(\theta) = \mathrm{CT}(0) - 9.205 \cdot 10^{-5} \cdot \theta + 2.042 \cdot 10^{-3} \cdot \theta^2 \quad (12)$$

where θ is trim in degrees, positive by bow.

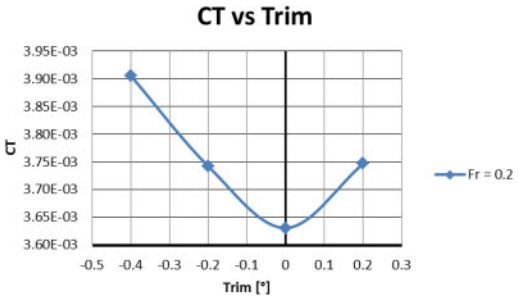

Figure 8. CT against initial trim.

Table 10. CT as function of Fr and draft.

Draft m	Fr = 0.20
0.12 (min)	4.018e−03
0.144 (mid)	3.924e−03
0.168 (design)	3.631e−03

Table 11. Wet surface and longitudinal position of G for every draft.

Draft m	S m^2	xG m
0.12 (min)	2.134	−0.060
0.144 (mid)	2.440	−0.097
0.168 (design)	2.788	−0.140

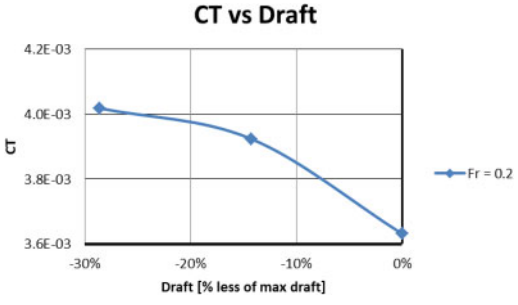

Figure 9. CT against initial draft.

5.2 *Draft effects*

The minimum draft allowed corresponds to the complete immersion of the propeller disc; the intermediate draft is an average between this and the design one, considered as the maximum allowed.

Remember that in this case, against the trim one, the wet surface changes significantly for every draft so the *S* used to obtain the non-dimensional form changes for each case.

In following plot drafts are reported as fraction of design draft (considered as maximum).

A second order dependence of the resistance from the draft has been observed, with the minimum value

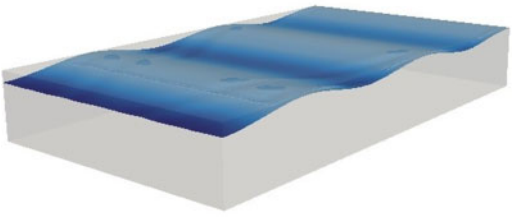

Figure 10. Wave pattern that appears at higher Fr numbers (amplified for illustration purposes).

for the design condition. Polynomial fit has been constructed for CT dependence from draft, as shown in Eq. (13).

$$CT(T) = \mathrm{CT(Td)} + 2.747 \cdot 10^{-3} \cdot T - 4.876 \cdot 10^{-3} \cdot T^2 \quad (13)$$

where T is a fraction of design draft (0 is design draft, −0.5 is half of design draft).

6 RESULTS AT HIGHER FR NUMBERS

As pointed before, the model set up for Fr = 0.20 does not work for higher Fr numbers. This is supposed to happen due to the fact that the wave pattern not dissipates completely before the outlet, reflecting and producing waves from the inlet. A much longer domain would be required, but this implies also a substantial increase of cells number that at this stage is being avoided.

Simulation without the ship has been performed in order to check if wave from the inlet are related only to the Kelvin pattern or they're caused by other reasons. It's been checked that, at higher fluid velocity, waves are present as well (Figure 10), so the problem is supposed to be related to the outlet boundary conditions or the solution schemes.

The problem has been avoided forcing a dynamic pressure boundary condition at the outlet, setting it to zero. That is equal to say that all the flow perturbations are exhausted when they reach the outlet, and it is not physically true. However, this avoids the creation of the wave pattern of Figure 10 and allows simulations reach convergence.

The implicit incorrectness of this model set up leads to results not very reliable. This model set up has been used to repeat runs at Fr = 0.2 and the results have been compared to those shown in section 5. Due to the implicit incorrectness of this new model set up, a coarse mesh has been used in order to save computational time.

Refinement across the free surface has been performed, but at a lower level than that one performed before; features of this new mesh are reported in Table 2. Comparison shows significant differences between the two approaches, as pointed in Table 12 and Table 13, so even if simulations have shown convergence results haven't been considered reliable. Further investigation in this field is required.

Table 12. Setup comparison, static mesh.

	Static mesh LTSInterFoam	Static mesh interFoam
Fr	0.20	0.20
U, m/s	1.1885	1.1885
Time step	Fixed (1e−3)	Adjustable
Total cells	1328903	733974
P_rgh BC (outlet)	zeroGradient	fixedValue (0)
Iterations	15000	8000
CT	3.631e−03	4.462e−03
Sinkage, %	0.60	2.02
Trim, deg	0.104	0.075

Table 13. Setup comparison, dyamic mesh.

	Dynamic mesh interDyMFoam	Dynamic mesh interDyMFoam
Fr	0.20	0.20
U, m/s	1.1885	1.1885
Time step	Adjustable	Adjustable
Total cells	1328903	733974
P_rgh BC (outlet)	zeroGradient	fixedValue (0)
Iterations	65000	10000
CT	3.634e−03	6.331e−03
Sinkage, %	1.45	1.88
Trim, deg	−0.109	−0.073

7 CONCLUSIONS

Bare hull resistance of a ropax has been calculated with numerical simulation run in OpenFOAM. Various Fr numbers, trim angles and drafts have been considered. Due to lack of experimental data, initial comparison with another well validated RaNS code has been performed in order to check the goodness of the results.

As first step, has been observed that the even keel resistance calculation in OpenFOAM is more reliable if done with a dynamic mesh able to sink and trim. Using interDyMFoam handling a dynamic mesh is recommended for resistance evaluation at design point and, as well, in design steps that require more precision. However, much time and computational power is needed to deal with dynamic mesh, so in an early stage a static mesh approach can be used to evaluate hull resistance as well as insights regarding the dependence of resistance by fixed trim angles and drafts. The LTSInterFoam solver is able to reach convergence quickly on a mid-refined mesh, so it's a useful tool for this kind of investigations. Influence of trim and draft at Fr = 0.2 has been found, evaluating also a regression

just as pointed in sections 5.1 and 5.2. The same analysis at higher Fr number have not been run successfully and further investigation will be necessary.

ACKNOWLEDGMENTS

The work is a part of the SHOPERA (Energy Efficient Safe SHip OPERAtion) collaborative project which is co-funded by the Research DG of the European Commission within the RTD activities of the FP7 Thematic Priority Transport/ FP7-SST-2013-RTD-1.

REFERENCES

Ahmed, Y. and Guedes Soares, C. Simulation of Free Surface Flow around a VLCC Hull using Viscous and Potential Flow Methods. *Ocean Engineering.* 2009; 36(9–10): 691–696.

Campana, E.F., Peri, D., Tahara, Y., Stern, F., 2006. Shape optimization in ship hydrodynamics using computational fluid dynamics. *Computer methods in applied mechanics and engineering 196:* 634–651.

Carrica, P.M., Fu, H., Stern, F., 2011. Computations of self-propulsion free to sink and trim and of motions in head waves of the KRISO Container Ship (KCS) model. *Applied Ocean Research 33:* 309–320.

Ciortan, C., Wanderley, J., Guedes Soares, C., 2007. Turbulent free-surface flow around a Wigley hull using the slightly compressible flow formulation. *Ocean Engineering 34:* 1383–1392.

Ciortan, C., Wanderley, J.B.V., Guedes Soares, C., 2012. Free surface flow around a ship model using an interface-capturing method. *Ocean Engineering 44*: 57–67.

Galli, A.M., Gualeni, P., Stranieri, G., Qualich, S., Cusano, G., 2014. Monitoring and analysis of the performance data of a RO-PAX ship in the perspective of energy efficiency. *Polish Maritime Research 4(84) Vol. 21:* 18–26.

Haack, T., Krüger, S., Vorhölter, H., 2009. Optimization of a fast monohull with CFD-methods. *10th International Conference on Fast Sea Transportation (FAST),* Athens.

Hajivand, A., Mousavizadegan, S.H., 2015. Virtual maneuvering test in CFD media in presence of free surface. *Int. J. Nav. Ocean. Eng. 7:* 540–558.

Higuera, P., Lara, J.L., Losada, I.J., 2013. Realistic wave generation and active wave absorption for Navier-Stokes models application to OpenFOAM. *Coastal Engineering 71*: 102–118.

Hu, Z., Tang, W., Xue, H., Zhang, X., Guo, J., 2015. Numerical simulations using conserved wave absorption applied to Navier-Stokes equation model. *Coastal engineering 99*: 15–25.

Islam, H., Akimoto, H., 2015. Prediction of ship resistance in Head Waves Using RaNS based solver. *13th International Conference on Mechanical Engineering (ICME)*, BUET.

ITTC, 2011. Pratical guidelines for ship CFD applications. In:*Recommended procedure and Guidelines.*

Jackson, A., 2012. A comprehensive tour of snappyHexMesh. *7th OpenFOAM workshop,* Darmstadt.

Jin, Y., Duffy, J., Chai, S., Chin, C., Bose, N., 2016. URANS study of scale effects on hydrodynamic maneuvering coefficients of KVLCC2. *Ocean Engineering 118:* 93–106.

Kim, H., Akimoto, H., Islam, H., 2015. Estimation of the hydrodynamic derivatives by RaNS simulation of planar motion mechanism test. *Ocean Engineering 108:* 129–139.

Löhner, R., Yang, C., Oñeto, E., Idelssohn, S., 1999. An unstructured grid-based, parallel free surface solver. *Applied Numerical Mathematics 31:* 274–293.

Maki, K., 2011. Ship resistance simulation with OpenFOAM. *6th OpenFOAM workshop.* The Pennsylvania State University, USA.

Maki, K., Broglia, R., Doctors, L.J., Di Mascio, A., 2013. Numerical investigation of the components of calm-water resistance of a surface-effect ship. *Ocean Engineering 72*: 375–385.

Mordhorst, C.J., 2011. Investigation of open-source CFD software on shipyards. Thesis, Chalmers University of technology.

Orihara, H., Miyata, H., 2003. Evaluation of added resistance in regular incident waves by computational fluid dynamics motion simulation using an overlapping grid system. *Journal of Marine Science and Technol (2003) 8:* 47–60.

Prever, R., Grabert, R., 2004. Improving fuel efficiency in Ro-Pax design. *RoRo 2004 Exhibition and Conference – the International RoRo Event from Ship to Shore,* Goeteborg.

Shi, A., Wu, M., Yang, B., Wang, X., Wang, Z., 2012. Resistance calculation and motions simulation for free surface ship based on CFD. *Procedia Engineering 31:* 68–74.

Percival, S., Hendrix, D., Noblesse, F., 2001. Hydrodynamic optimization of ship hull forms. *Applied Ocean Research 23:* 337–355.

Peri, M., Rossetti, M., Campana, E.F., 2001. Design optimization of ship hulls via cfd techniques. *Journal of ship research 45:* 140–149.

Tarbiat, S., Lavrov., A., Guedes Soares, C., 2014. Numerical simulation of the free surface turbulent flow of a Wigley hull with trim and drift angle. Guedes Soares, C. & Santos T.A. (Eds.). *Maritime Technology and Engineering.* Taylor & Francis Group, UK: 1009–1018.

Wooliscroft, M.O., Maki, K.J., 2016. A fast-running CFD formulation for unsteady ship maneuvering performance prediction. *Ocean Engineering 117*: 154–162.

Wortley, S., 2013. CFD analysis of container ship sinkage, trim and resistance. Thesis, Curtain University.

Yang, C., Löhner, R., Noblesse, F., Huang, T.T., 2000. Calculation of ship sinkage and trim using unstructured grids. *European Congress on Computational Methods in Applied Sciences and Engineering (ECCOMAS 2000),* Barcelona.

Yang, C., Huang, F., Wang, L., 2011. Numerical simulations of highly nonlinear steady and unsteady free surface flows. *Journal of Hydrodynamics 23(6)*: 683–696.